Applied Surface Science 337 (2015) 72–80

Contents lists available at ScienceDirect

Applied Surface Science

journal homepage: www.elsevier.com/locate/apsusc

Synthesis, structural characterisation and antibacterial activity of Ag^+-doped fluorapatite nanomaterials prepared by neutralization method

Vojislav Stanić[a,*], Ana S. Radosavljević-Mihajlović[a], Vukosava Živković-Radovanović[b], Branislav Nastasijević[a], Milena Marinović-Cincović[a], Jelena P. Marković[a], Milica D. Budimir[a]

[a] University of Belgrade, Vinča Institute of Nuclear Sciences, P.O. Box 522, 11001 Belgrade, Serbia
[b] University of Belgrade, Faculty of Chemistry, P.O. Box 51, 11158 Belgrade, Serbia

ARTICLE INFO

Article history:
Received 27 November 2014
Received in revised form 8 January 2015
Accepted 6 February 2015
Available online 16 February 2015

Keywords:
Fluoroapatite
Silver
Biomaterials
Antibacterial
Neutralization method

ABSTRACT

Silver doped fluorapatite nanopowders were synthesised by neutralization method, which consists of dissolving Ag_2O in solution of HF and H_3PO_4 and addition to suspension of $Ca(OH)_2$. The powder XRD, SEM and FTIR studies indicated the formation of a fluorapatite nanomaterials with average length of the particles is about 80 nm and a width of about 15 nm. The FTIR studies show that carbonate content in samples is very small and carbonte ions substitute both phosphate and hydroxyl groups in the crystal structure of samples, forming AB-type fluorapatite. Antibacterial studies have demonstrated that all Ag^+-doped fluorapatite samples exhibit bactericidal effect against pathogens: *Staphylococcus aureus*, *Micrococcus luteus* and *Kllebsiela pneumoniae*. Antibacterial activity increased with the increase of Ag^+ in the samples. The atomic force microscopy studies revealed extensive damage to the bacterial cell envelops in the presence of Ag^+-doped fluorapatite particles which may lead to their death. The synthesized Ag^+-doped fluorapatite nanomaterials are promising as antibacterial biomaterials in orthopedics and dentistry.

1. Introduction

Biomaterials based on hydroxyapatite (HAP; $Ca_{10}(PO_4)_6(OH)_2$) are commercially available for the repair and reconstruction of bone tissue defects [1,2]. Synthetic hydroxyapatite is very similar with inorganic component of bone and exhibited bioactivity, biocontability, osteoconductivity and no toxicity. The application of hydroxyapatite could come in different forms like powder, granules and coatings of metal implants and polymer composites. Orthopedic implant infections are significant because of their morbidity and usually require the removal or replacement of installed materials [3]. Incorporation of antibacterial agents such as antibiotics, fluorine and biocides metal ions; in the implant biomaterial alone proved to be very successful in the prophylaxis [4]. Dental restorative materials that release fluoride ions have been noted to very effective in the prevention of caries [5]. Fluoride ions have a weak bactericidal effect, but in combination with silver, the effect is very pronounced. Compounds such as, AgF and $Ag(NH_3)_2F$ are very efficient in the prevention and treatment of dental caries [5–8]. Silver ions have expressed an oligodynamic property with negligible cytotoxic effects on human cells. High concentrations of silver ions can be cytotoxic and cause argyria [9,10]. Hydroxyapatite doped with small amounts of silver ions showed a broad spectrum of antibacterial activity and the absence of cytotoxicity [11–13].

Fluorapatite (FAP; $Ca_{10}(PO_4)_6F_2$) is considered as potential biomaterial for bone repair due to bioactive and biocompatible and antibacterial activity [14–18]. It is structurally and chemically similar to hydroxyapatite, but it has better physic-chemical stability such as lower solubility in acidic medium. In vivo studies are showed that fluorapatite material had osteoconductive properties [19]. In vitro studies have showed that the cytotoxic, genotoxic and mutagenic effects of fluorapatite and fluorhydroxyapatite materials have no effect or are negligible [20–22]. Several studies are showed that FAP materials have antibacterial activities but not the biocidal effect [15–18]. Low solubility of FAP in acidic media makes it suitable antibacterial material for a longer period of time.

* Corresponding author.
E-mail address: voyo@vinca.rs (V. Stanić).

http://dx.doi.org/10.1016/j.apsusc.2015.02.065
0169-4332/

Various metal ions, such as: Ag^{+}, Cu^{2+}, Zn^{2+}, Ce^{3+}, Eu^{3+}, Sr^{2+}, Ga^{3+}, Ti^{4+} and Co^{2+}; have been used to doped hydroxyapatite biomaterials with in order to get antibacterial activity [11–13,23–25]. In vitro studies have showed that silver doped hydroxyapatite materials have no significant cytotoxic activity [13,26,27].

There are few reports of synthesis of silver doped fluorapatite by electrochemical deposition and coprecipitation method [28–30]. In all reports sintered Ag-doped samples showed high antibacterial activity.

Another potential application of antibacterial materials based on silver-apatite materials is their use for water disinfection [31].

Various methods have been developed for the preparation of fluorapatite, such as neutralization, precipitation, sol–gel processing, mechanochemical synthesis, microwave and flame spray pyrolysis; [17,18,32–36]. Synthesis of fluorapatite by neutralization chemical method can be represented by the following Eq. (1) [18]:

$$10Ca(OH)_2 + 6H_3PO_4 + 2HF = Ca_{10}(PO_4)_6F_2 + 10H_2O \quad (1)$$

Neutralization method is very simplicity, the pure product is obtained and suitable for industrial production. Many synthesis parameters, such as: reactant concentration, aging time, temperature, have an influence on the properties of the obtained hydroxyapatite precipitate [37]. Titration $Ca(OH)_2$ suspension with a solution of H_3PO_4 and HF to pH 7 and a long period of aging of precipitate, allows almost complete incorporation of fluoride ions [18].

In the present study, as model compounds were synthesized and characterized fluorapatite materials doped with different amounts of silver ions, by neutralization method. The antimicrobial effects of synthesized samples are evaluated against pathogens: *Staphylococcus aureus* (*S. aureus*), *Micrococcus luteus* (*M. luteus*) and *Kllebsiela pneumoniae* (*K. pneumoniae*). Special emphasis was made on the influence of synthesized materials on the morphology of the tested microorganisms.

2. Materials and methods

2.1. Preparation of the materials

Synthesis of FAP and Ag^{+}-doped FAP powders were performed according to the neutralization method as described in our previous work [18]. Starting chemicals used for the synthesis of powders were: $CaCO_3$ (Merck, min. 98.5%,), Ag_2O (Merck, 99+%,), HF (VWR BDH Prolabo, min. 48%) and H_3PO_4 (VWR BDH Prolabo, min. 85%). CaO was obtained by calcinations of $CaCO_3$ for 20 h at 1000 °C. Experiments were performed in an air atmosphere. Double distilled water was used throughout all the experiments. All Ag^{+}-doped FAP samples were synthesized with the amount (Ag + Ca) = 0.125 mol. Atomic ratios of [Ag/(Ag + Ca)]·100% in the range 0–1%, with the constant ratio (Ag + Ca)/P were fixed at 1.67. The compositions of the starting materials are given in Table 1. The $Ca(OH)_2$ suspension was prepared by stirring (at a rate of 300 rpm) a required amount of CaO into 250 mL water, heated to 70 °C. A required amount of Ag_2O was dissolved in 150 mL of 0.5 M H_3PO_4 and 0.167 M HF. Then the solution was added dropwise at rate of about 1–2 mL min^{-1} to a suspension of $Ca(OH)_2$ (stirred at a rate of 300 rpm) until the end point is reached (pH 7). After titration and maturation (16 h, at rate of 200 rpm) at room temperature (20 °C), apatite suspensions are filtrated in a Buchner funnel, dried at 105 °C and pulverized into powder.

Table 1
The results of chemical analyses of FAP and AgFAP samples.

Sample	(Ag + Ca)/P	Ag/(Ag + Ca), (%)		F, (%)	
		Nominal	Measured	Nominal	Measured
FAP	1.69	–	–	100	101.4
AgFAP1	1.79	0.01	0.009	100	98.9
AgFAP2	1.76	0.1	0.097	100	99.4
AgFAP3	1.85	1	1.024	100	100.3

2.2. Characterization of synthesized apatite samples

The XRPD patterns were obtained on a Simens D500 automated diffractometer using a Cu tube operated at 35 kV and 20 mA. The XRPD data were collected by using the step scanning mode in the range of Bragg angle $2\theta = 4–70°$ at each 0.02 step counting for 1 s. For identification of the mineral composition were used JCPDS database and software program PCPDFWIN. For processing the X-ray powder diagram was used the program Powder Cell 2.4 [38].

The FTIR spectra of synthesized apatite samples, were recorded by a Nicolet 6700 FTIR spectrophotometer (Thermo Scientific) using the ATR technique, in the frequency interval of 4000–400 cm^{-1}.

The field-emission scanning electron microscopy (FESEM) observations and measurements were performed using TESCAN Mira3 XMU at 20 kV. The apatite samples were previously sputtered and coated with Au–Pd alloy.

The thermal stability of the FAP and AgFAP3 samples was investigated by simultaneous non-isothermal thermo-gravimetric analysis (TGA) and differential thermal analysis (DTA) using a SETARAM SETSYS Evolution 1750 instrument. The measurements were conducted at a heating rate of 10 °C/min in a dynamic argon atmosphere (flow rate was 20 cm^3/min) in the temperature range of 30–1200 °C.

The quantitative analysis of Ca and P were determined by ICPOES Thermo iCAP 6500, while amount of Ag determined by ICPMS Thermo iCAPqICP. Fluorine was determined by selective ion electrode system.

Nitrogen adsorption–desorption isotherms were determined using a Micromeritics ASAP 2020 instrument. Samples were degassed at 110 °C for 10 h under reduced pressure. The specific surface area of samples was calculated according to the Brunauer, Emmett, Teller (BET) method from the linear part of the nitrogen adsorption isotherms. The total pore volume (Vtot) was given at $p/p0 = 0.998$. The volume of the mesopores was calculated according to the Barrett, Joyner and Halenda method from the desorption branch of isotherm. The volume of micropores was calculated from alpha-S plot.

2.3. Ions release test

The 0.3 g FAP or Ag^{+}-doped FAP was placed in plastic bottles that were filled with 30 mL of phosphate buffer solution (pH 7.2). The phosphate buffer pH 7.2 composed of KH_2PO_4 (0.133 M) and Na_2CO_3 (0.048 M). The bottles were shaken for 0.5, 1 and 2 h at 37 °C in a shaking water bath. After the required time, the Ag^{+} concentrations in the solutions were then measured by inductively coupled plasma (ICP) spectrometry and selective ion electrode system.

2.4. In vitro Antibacterial investigations of Ag-doped fluorapatite nanopowders

2.4.1. Materials

Culture media: LAB 8 nutrition agar (Lab M, Bury, United Kingdom). 0.133 M phosphate buffer solution (PBS), pH 7.2 was made by dissolving in deionized water 18.100 g of KH_2PO_4 and 5.035 g of Na_2CO_3 (p.a. grade, Merck, Darmstadt, Germany) in a liter volumetric flask. Final pH 7.2 ± 0.2 is taken after buffer has been autoclaved and cooled to room temperature.

2.4.2. Antibacterial activity test

Samples were in vitro investigated for their antibacterial activity against *K. pneumoniae* NCIMB 9111, *S. aureus* ATCC 25923 and *M. luteus* ATCC 4698. The strains were cultivated on agar slants on 37 °C in thermostat for 24 h.

Microbiological challenge study was performed according to described method [25] with some modifications. Initial bacterial inoculums (~10^{10} CFU/mL) was obtained by cell dispersion from the surface of well grown bacterial slant culture in 3.0 mL of the sterile buffer thermostated at 37 °C. Additional dilution of cell suspension was made with the thermostated PBS, too. A 100 mg of investigated apatite sample (sterilized in the tube at 180 °C for two hours) was challenged to 10 mL of appropriate bacterial suspension. Each tube vas immediately vigorously vortexed dozen seconds before 0.100 mL aliquot for initial time viable cell determination has been taken. Tubes were placed in thermostat during the experiment. Every 10 min tubes were vigorously vortexed. 0.100 mL aliquots were taken in definite time periods and 10 fold diluted with 0.9 mL of sterile buffer in microtubes to required extent. 1 mL of the last dilution was used for viable cell determination as colony-forming units (CFU/mL) by mixing in a small Petri dish with 5 mL of molten nutrition agar and thermostating for 24 h (48 h for *M. luteus*). In the case of *S. aureus* bacterial suspension contained 3.7×10^6 CFU/mL for *K. pneumoniae* was 3.3×10^6 CFU/mL and for M. luteus was 2.9×10^6 CFU/mL and incubation during challenge testing took two hours. As controls, the buffer was also challenged to chosen strains the appropriate time. Challenge experiments were repeated three times for each culture, and average values were taken as the results.

The percentage of microorganism reduction (R) was calculated using Eq. (2):

$$R\% = 100 \times (C_0 - C)/C_0 \quad (2)$$

were C_0 is the average number of the strain colonies of the control and C is the corresponding number of colonies of challenged apatite samples at the same predetermined time.

The mean value and standard deviation were calculated using the Origin Pro software (OriginLab Corporation).

2.5. Sample preparation for AFM imaging

S. aureus, *K. peneumoniae* and *M. luteus* bacteria were suspended from nutritional broth in PBS (pH 7.2). The number of cells in the suspension was ~10^{10} CFU/mL. Incubation of bacteria with AgFAP3 was performed in eppendorf tubes (2 mL) where 10 mg of sample were added, followed by 300 μL of PBS and 300 μL of bacterial suspensions. These suspensions were mixed shortly at vortex and placed at shaker for 5, 10 and 15 min. The same procedure was used for controls, performed for each tested bacteria, without adding of AgFAP3. After incubation, AgFAP3 was separated from bacteria using short spinning. Supernatant with treated bacteria and controls were transferred in eppendorfs, then mixed with 600 μL of 5% glutaraldehyde (v/v in PBS) and left at least 1 h at room temperature. After incubation with glutaraldehyde, bacterial suspension were centrifuged at 13,000 rpm using Eppendorf centrifuge. Bacterial pellets obtained were washed three times with 0.85% (v/v) saline solution and resuspended in 100 μL of PBS. Such prepared bacterial cells were used for AFM imaging.

A single monolayer thin film of small aliquots of each sample was deposited on mica substrate by spin coating and imaged after drying at room temperature. Surface topography of cells was observed by atomic force microscopy (AFM). AFM measurements were performed using a Quesant AFM (Aguora Hills, CA) operating in tapping mode in air on room temperature, with standard silicone tips (NanoAndMore Gmbh, Wetzlar, Germany) and with the constant force of 40 N/m.

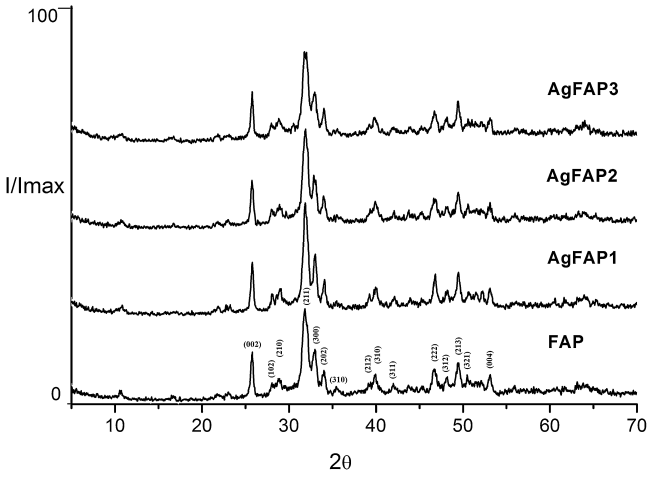

Fig. 1. XRD patterns of the as-prepared powders with different silver concentrations.

3. Results

3.1. Characterization of fluorapatite nanocrystals

The XRD patterns of FAP and Ag^+-doped FAP samples are presented in Fig. 1. The positions of its X-ray diffraction peaks were in accordance with ASTM data for fluorapatite (Card 15-0876). The patterns of the synthesized Ag doped fluorapatite samples are similar with pure fluorapatite. Lattice parameters a, b and c, crystallite size of samples are presented in Table 2.

The FTIR spectra of each of the samples contain characteristic bands of apatite compounds (Fig. 2). The phosphate bands are observed at about 960 cm^{-1} (ν_1) 1033 cm^{-1} (ν_3) and shoudler at about 1095 cm^{-1} (ν_3), while doublet present at around 601–561 cm^{-1} (ν_4). The broad band at 2500 cm^{-1}–3700 cm^{-1} and a small band at about 1650 cm^{-1} were associated with water absorbed and present in the samples. The small band at about 1650 cm^{-1} (ν_3) is ascribed to CO_3^{2-} ions. Samples doped with silver ions contain additional bands of low intensity originating from the CO_3^{2-} ions at about 755 cm^{-1} (ν_4), 877 cm^{-1} (ν_2) and 1555 cm^{-1} (ν_3).

Fig. 3 shows the morphology of FAP and Ag^+-doped samples. The morphology of powders indicates that each of them is composed of agglomerates which consist of particles with irregular rod-shape and wide size distributions. The prepared fluorapatite nanomaterials have an average length of particles of about 80 nm and a width of about 15 nm. In the samples can also be seen particles of smaller size as well as those that are longer than 100 nm.

The results of elemental analysis of all synthesized samples are summarized in Table 1.

Fig. 4 shows the curves of TGA and DTA of FAP and AgFAP3 samples. Appearance and position of the peaks in the DTA and TGA

Table 2
Unit cell parameters and crystallite sizes (X_s) of FAP and Ag^+-doped samples.

Sample	Unit cell parameters (Å)		X_s
	a	*c*	
FAP	9.3672	6.8729	43
AgFAP1	9.3720	6.8744	31
AgFAP2	9.3794	6.8791	38
AgFAP3	9.3854	6.8844	39

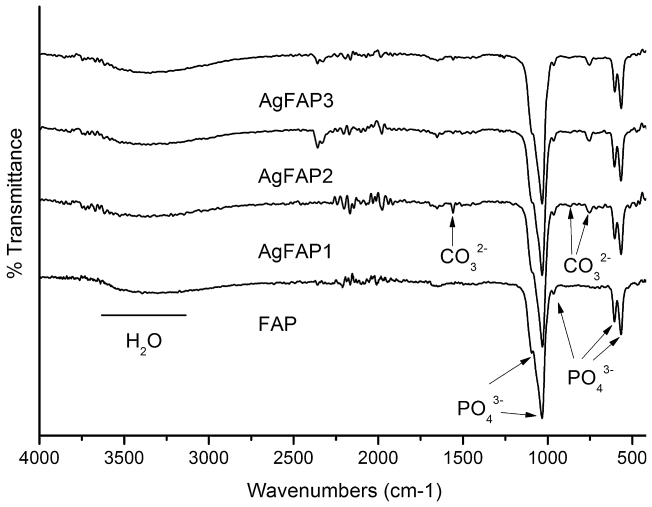

Fig. 2. FTIR transmittance spectra of synthesized samples: FAP, AgFAP1, AgFAP2 and AgFAP3.

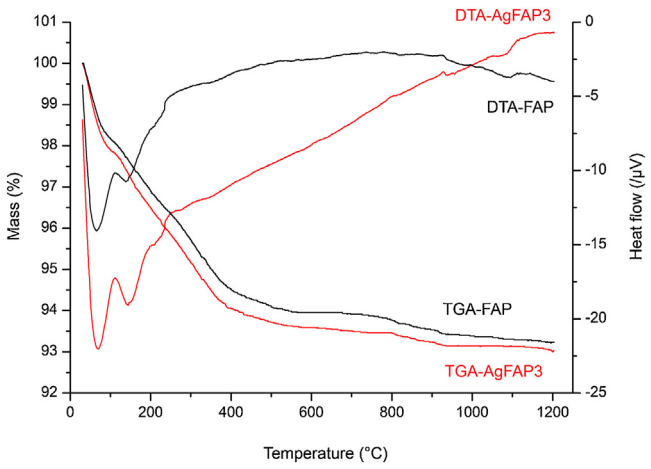

Fig. 4. TGA and DTA curves of FAP and AgFAP3 samples.

curves of both samples are similar. The TGA curves show three-stage weight loss at the temperature ranges about of 30–84 °C, 84–550 °C and 743–922 °C. The first stage of weight loss for each sample was about 2%, second about 4% and third about 0.4%. The DTA curves contains three endothermic peaks maxima are observed at about 70 °C, 145 °C and 1080 °C.

Fig. 5 shows the N_2 adsorption/desorption isotherms of AgHAP3 powder. Isotherms other samples are very similar with this one. It can be seen that isotherm have typical H1-hysteresis loops, which demonstrate the properties of typical mesoporous materials.

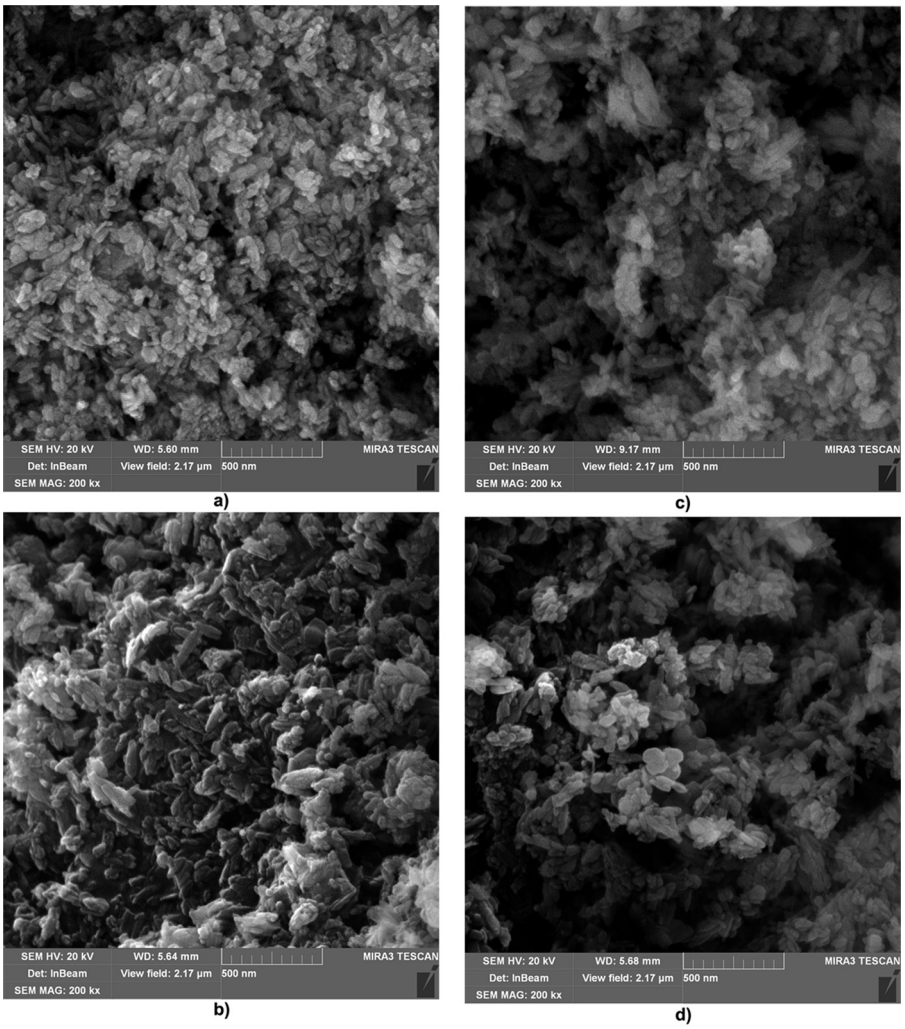

Fig. 3. Scanning electron micrograph of FAP (a); AgFAP1 (b), AgFAP2 (c) and AgFAP3 (d).

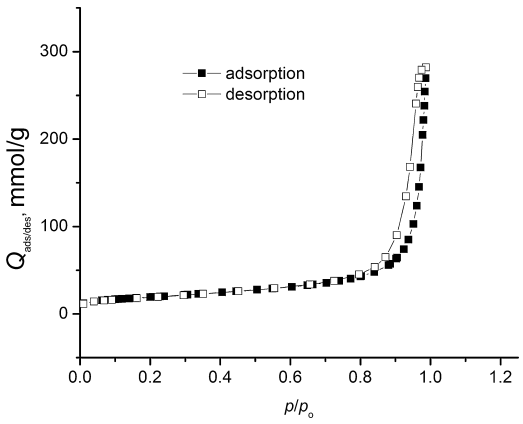

Fig. 5. N_2 adsorption–desorption isotherms of AgFAP3 sample.

The dependence of specific surface area on the amount of silver ions in fluorapatite samples is displayed Table 3. All the synthesized powders show a specific surface area about 60 m^2/g.

3.2. Dissolution properties

The amounts of released Ag^+ and F^- ions in PBS (pH 7.2) from synthesized samples are shown in Fig. 6.

3.3. The results of antibacterial activity determination

The antibacterial effect of the Ag^+-doped FAP samples against *K. Pneumoniae*, *S. aureus* and *M. luteus* are shown in Fig. 7. The antibacterial efficiency of samples is a function of quantities of silver ions, exposure time as well as of strain bacterium. The sample with the highest content of silver ions has killed all the *K. pneumoniae* and *M. luteus* cells after 1 h of exposure and reduce the number of *S. aureus* cells by 99.57% after 2 h.

3.4. Morphological changes of bacteria after treatment with AgFAP3 nanoparticles

Morphological characterization of the untreated *S. aureus* cell, showed typically spherical shape, with smooth surface (Fig. 8a). The treatment of *S. aureus* with AgFAP3 (Fig. 8b) caused distortion of the round shape of the cell and the appearance of vesicle. Fig. 7c shows the typical near-spherical shaped form of a single M. luteus cell before exposure to AgFAP3 nanoparticles. After exposure, in Fig. 8d can be seen damage to the cell envelope in the form of vesicle. The surface of the untreated *K. pneumoniae* cell (Fig. 8e) was covered by highly wrinkled structures. Fig. 9f showed two assembled cells of *K. pneumoniae* treated with AgFAP3 particles. On the cells surface the damage is visible in the form of blisters.

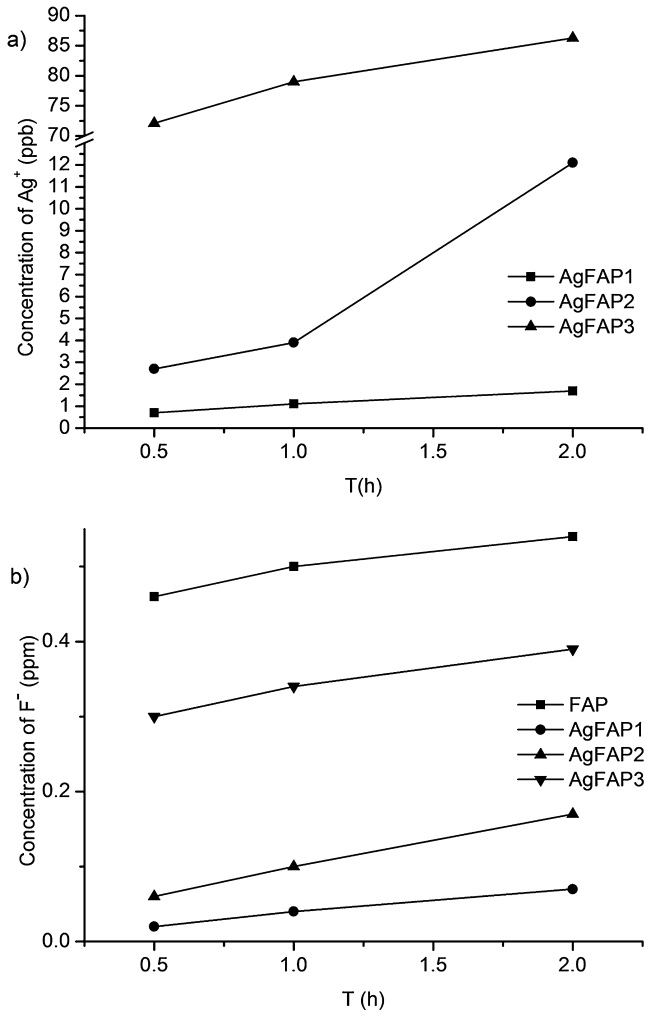

Fig. 6. The concentration of released Ag^+ and F^- from FAP and AgFAP samples during the immersion time in PBS (pH 7.2).

4. Discussion

The neutralization method is very suitable for obtaining monophase antimicrobial Ag^+, Cu^{2+} and Zn^{2+} doped hydroxyapatite materials, based on the dissolution of metal oxides in H_3PO_4 [13,25]. In this paper, we Ag_2O dissolved into a mixture of H_3PO_4 and HF and slowly added to the Ca $(OH)_2$ suspension in order homogeneous distribution of silver ions. Apatite obtained by neutralization method are very suitable for medical researches.

The XRD patterns of the synthesized Ag^+-doped fluorapatite samples are similar with pure fluorapatite. All of the diffraction peaks were broad, indicating the obtained crystallites were nanosized. There are no other characteristic peaks of impurities,

Table 3
The specific surface area and pore volume of FAP and AgFAP powders.

Sample	S_p (m2/g)	V_{total} (cm^3/g)	V_{meso} (cm^3/g)	V_{micro} (cm^3/g)	D (nm)	D_{max} (nm)
FAP	56.70	0.3442	0.3427	0.0174	22.74	31.00
AgFAP1	64.09	0.3574	0.3557	0.0199	20.94	26.80
AgFAP2	60.35	0.3359	0.3337	0.0189	21.44	32.10
AgFAP3	65.84	0.3833	0.3823	0.0210	22.74	31.30

S_p – specific surface.
V_{total} – total pore volume.
V_{meso} – volume of mesopores, the pores between 1.7 and 300 nm.
V_{micro} – volume of micropores.
D – average diameter of pores.
D_{max} – diameter of pores with the largest volume.

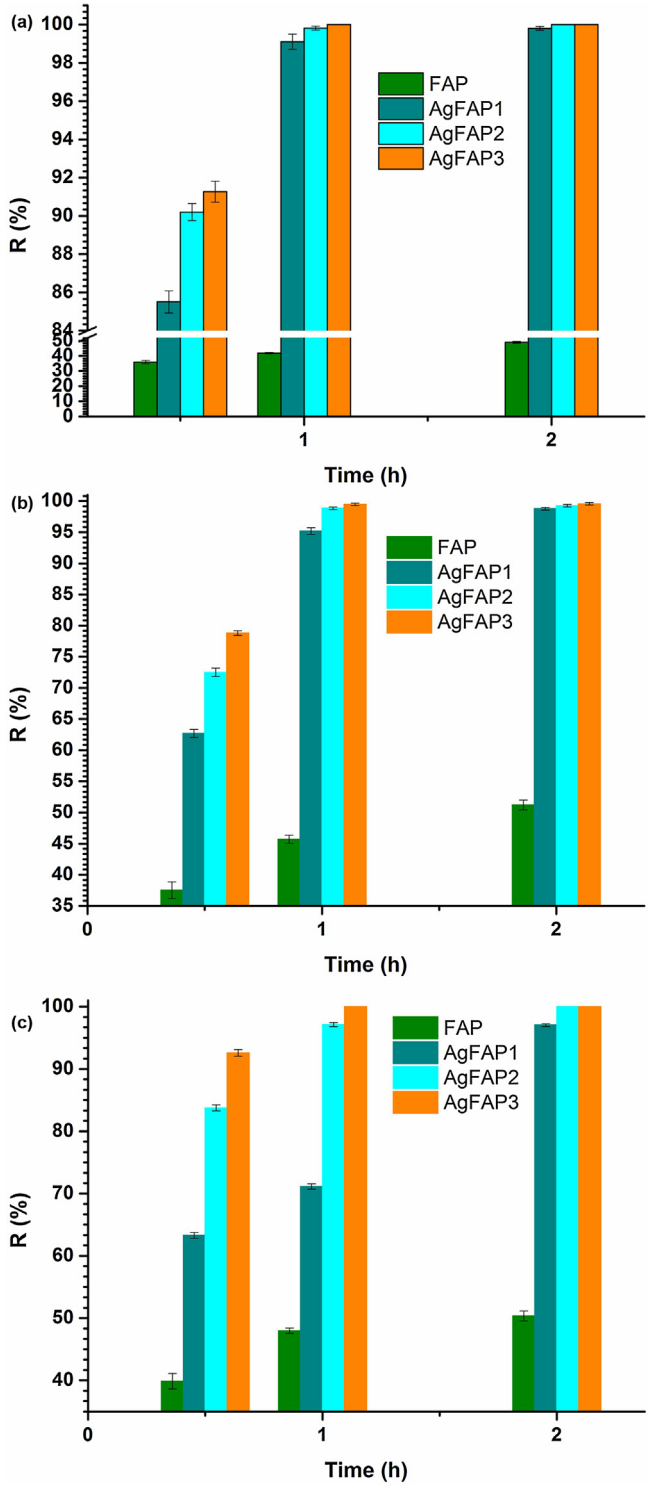

Fig. 7. The percentage of bacterial reduction (R%) for (a) *K. pneumoniae*, (b) *S. aureus* and (c) *M. luteus* after the treatment with the synthesized powders in time.

such as CaO, Ag_2O and silver phosphates. Doping of Ag^+ ions into the fluorapatite shows an increase in **a** and **c** lattice parameters (Table). A expansion of these lattice parameters may be caused by the substitution of bigger radius Ag^+ (0.128 nm) in Ca^{2+} (0.099 nm) ion in the FAP phase. It is also possible that the silver ions partially or completely not substitute calcium ions but occur in a special position, which modifies the crystalline environment. The silver ions causes a decrease in the size of the crystallites in doped samples (Table 2).

In the FT-IR spectrum (Fig. 2) of the all samples, the positions of the most relevant bands are in agreement with literature data [39]. The presence of a weak bands at 755 cm^{-1} and 877 cm^{-1} in Ag^+-doped fluorapatite samples, indicate to A-type of substitution which CO_3^{2-} groups replaces F^- groups [40]. The 1550 cm^{-1} band was assignable to CO_3^{2-} ions in PO_4^{3-} sites of the AgFAP1 crystals, B-type substitution [41]. The present absorptions indicate that the CO_3^{2-} group has substituted for bath F^- and PO_4^{3-} groups, indicates the formation of mixed AB-type carbonated fluorapatite structures. The weak carbonate band at about 1650 cm^- is assigned to surface carbonate ions, rather than those who are in the lattice of fluorapatite [41]. Based on the intensity of carbonate bands can be assumed that a small amount of incorporated in fluorapatite samples. The carbonate ions can also a influence on the lattice parameters values and the growth of apatite crystals in solution resulting in smaller crystals or even amorphous products.

Chemical analysis (Table 1) shows that all (Ag + Ca)/P ratios samples are the higher values than the amount of starting material. Fluoride content indicates that the obtained materials fluorapatite. The existing differences can be related to the presence traces of carbonate ions.

The thermal degradation properties of FAP and AgFAP3 are presented in Fig. 4. The results of the TGA-DTA analysis of FAP and AgFAP3 corresponded to the classical thermal behavior of fluorapatite [42]. There is no significant weight loss in the TGA curve of FAP and AgFAP3, as shown in Fig. 4. The FAP sample showed some better thermal stability than AgFAP3. The only difference between these two samples was found as a higher weight loss of AgFAP3 in the temperature range of 30–100 °C, compared to that of FAP. This was attributed to the location of free water in samples, which could not be removed by drying at room temperature. [42,43]. The second stage, 100–550 °C weight loss (4%) can also be attributed to the crystallization of the powders from the amorphous phase. Silver ions adversely affect the crystallization of fluorapatite, as a result of this it comes to reducing the size of crystallites (Table 2). In Fig. 4 the influence of silver ions on the crystallization of fluorapatite is not expressed, due to its very small amounts in AgFAP3. The third stage (743 °C–922 °C) weight loss of samples could influence the decarbonation and phase transformation. The temperature of decarbonation apatite decreases with an increase in the carbonate content. Natural carbonated fluorapatite begins to release CO_2 of about 800 °C for low carbonated samples, but heavily carbonated samples starting at lower temperatures of about 520 °C [44]. The consequence of decarbonation is the creation of FAP and CaO. The DTA curves contain three endothermic peaks maxima which are observed at about 70 °C, 145 °C and 1080 °C. The first two peaks in both curves correspond to the removal of adsorbed water and the third endothermic peak, at about 1080 °C in the DTA in both samples, indicates the formation of an eutectic between compounds formed during thermal decomposition. The nitrogen adsorption–desorption isotherm of AgHAP3 powder showed type IV isotherm and H1 hysteresis loop which indicated that all the synthesized materials mesoporous (Fig. 5). AgHAP3 sample exhibited hysteresis loops at $P/Po > 0.8$ due to its high surface area. The results of the nitrogen adsorption/desorption analysis (Table 3) indicates that the doping of Ag^+ has not altered the basic pore structure of FAP samples but improved the specific surface area for about 6–16%. Recently, Smiciklas et al. [37] have reported that lower temperature and shorter aging time obtained hydroxyapatites with larger specific surface area. Mesopores are usually formed during maturation due to the agglomeration of primary crystallites [45]. Mesoporous apatite biomaterials due to their high surface areas which are very significant for developing new types of bone implant, drug delivery systems and adsorbents. Biomaterials with larger pores exhibit better osseointegration and adsorption properties [46].

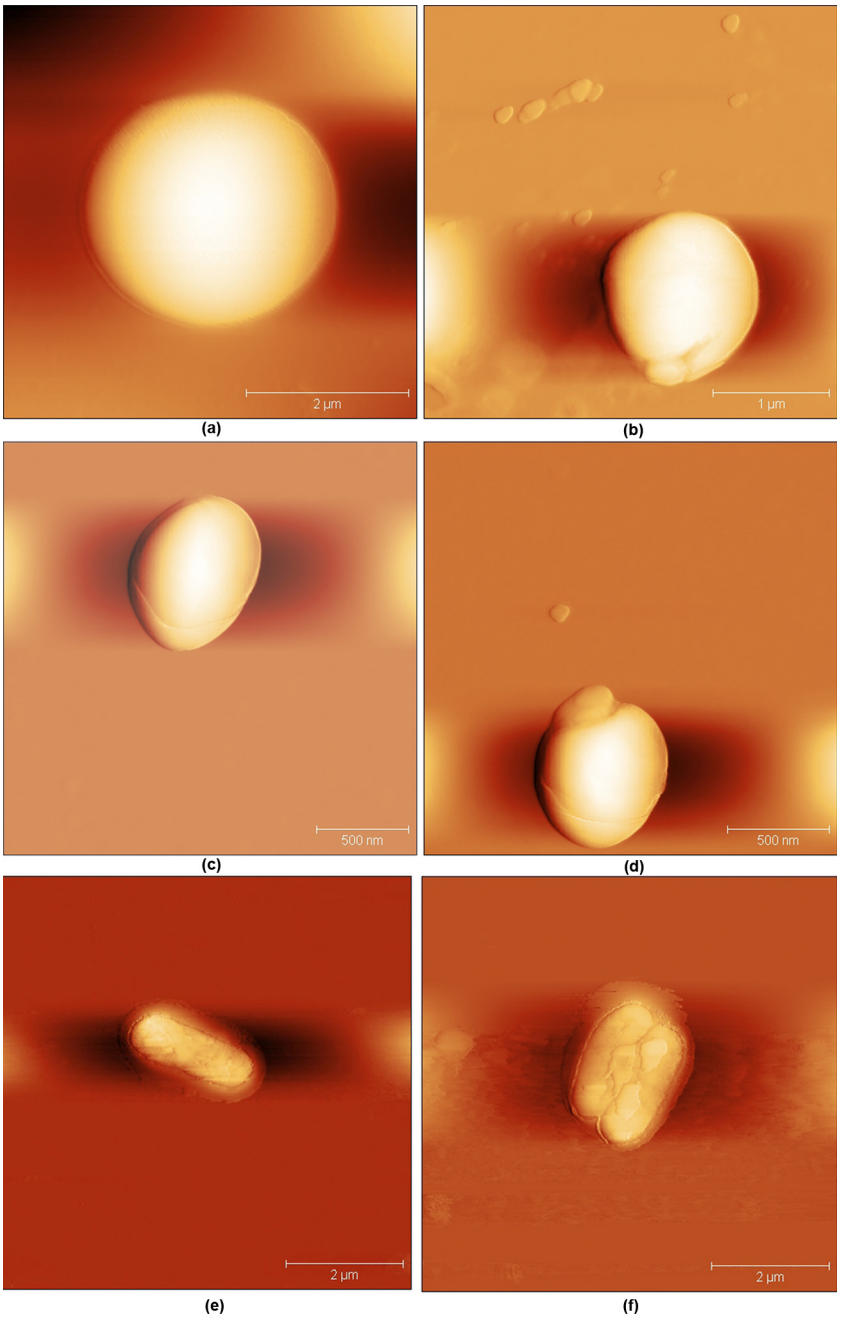

Fig. 8. AFM images of: *S. aureus* cells untreated (a); and treated with AgFAP3 particles (b); *M. luteus* cells untreated (c); and treated with AgFAP3 particles (d); and *K. pneumoniae* cells untreated (e); and treated with AgFAP3 particles (f).

Dissolution studies of prepared samples are a necessary to clarify the results of the antimicrobial tests and for assessing the suitability of their use. According to the results in Fig. 6 can concluded that the incorporation of silver ions into fluorapatite leads to increased rate of dissolution of AgFAP samples. Carbonate ions, particularly those present on the surface of the particles present in Ag doped fluorapatite samples likely affect the rate of release of fluoride ions. The silver and fluoride ions in the crystal surface of fluorapatite particles are thermodynamically unstable and can be relatively easily release into the surrounding environment. Dissolution process of apatite is regard to factors associated with properties of solution (pH, composition, saturation, temperature and hydrodynamics), bulk solid (chemical composition, crystallinity, particle sizes), and surface (specific surface area, defects, adsorbed ions) of apatite crystals [47]. The presence of carbonate ions and larger specific surface area increase the solubility of apatite materials.

The goal of antibacterial study was to investigate the potential of the synthesized materials against bacteria which can cause serious bone implant-related infections. The strains used in this study represented different types of bacteria Gram-negative *K. pneumoniae* and Gram-positive: *S. aureus* and *M. luteus* [48–50]. Among them, *S. aureus* is a major cause of bone infections. Bacteria shows an affinity that adhered to the surface of hydroxyapatite implants and it can lead to the formation of biofilm [51]. Bacteria in the biofilm can be propagated aggressively and resistance to antimicrobial therapy. Encapsulated bacteria show a particular tendency to over capsules adhere and form biofilms [51]. All tested bacteria can form biofilms and some of their strains possess a capsule. Fig. 8b and c clearly shows the existence of a capsule around *K. pneumoniae* cells.

According to the results of the antimicrobial assay (Fig. 7), FAP especially Ag^+-doped fluorapatites are very active against investigated bacterial species and cause great viable cell reduction in a relatively short time period of exposure. The FAP sample showed antibacterial activity against tested strains, the degree of reductions were about 50% after 2 h of exposure (Fig. 7). The reduction can associated with interaction bacterial cells and surfaces of FAP particle as well as with as well as with released fluoride ions. Previous studies have shown that use of fluoride either alone or in combination with other antibacterial agents has proved to be an effective in reducing the growth of cariogenic bacteria. Ge et al. reported that fluorhydroxyapatite coating on titanium showed antibacterial activity against *S. aureus*, *E. coli*, and *P. gingivalis* [16]. Antimicrobial activity of the fluorine substituted hydroxyapatite materials on *S. mutans* is a function of quantities of fluoride ions and pH value of the environmentals [51]. Fluorhydroxyapatite (FHA) presence in the polyetheretherketone/nano-FHA composite significantly reduces the adhesion and proliferation propagation of *S. mutans* on the surface [15]. Syed et al. [52] suggested that LiF exhibits a synergistic effect with a wide range of antibiotics reduced their minimal inhibitory concentration against clinical isolates of Gram-positive and Gram-negative bacteria including *K. pneumoniae*.

Among tested bacterial species, Gram-negative bacteria *K. pneumoniae* showed the greatest susceptible to AgFAP samples (Fig. 7a). AgFAP1 sample showed reduction ratio more than 85% after half an hour (0.5 h), while samples AgFAP2 and AgFAP3 had bactericidal effect after 2 and 1 h, respectively (Fig. 7a). Previously, Ciobanu et al. [53] reported that silver-doped hidroxyapatite nanoparticles show an efficient antibacterial activity against *K. Pneumoniae*. The Gram-positive bacteria *S. aureus* and *M. Luteus* were found to be slightly less sensitive to the AgFAP nanoparticles (Fig. 7b, c). This lower sensitivity can be attributed to the structural difference in cell envelope composition of Gram-positive and Gram-negative bacteria. We previously reported, that the *E. coli* (Gram-negative) bacteria showed greater sensitivity of *S. aureus* to silver-doped hydroxyapatite materials [13]. AgFAP1 sample against bath strains showed reduction ratio about 63% after half an hour of exposure. AgFAP3 sample reduced the number of *S. aureus* cells by 99.57% after 2 h (Fig. 7b). The AgFAP2 and AgFAP3 samples have killed all the *M. luteus* cells after the second and the first hour of exposure (Fig. 7c).

The antibacterial activity of AgFAP samples was confirmed by AFM analysis, where morphological disruption of bacterial cells were clearly seen. The morphological features of untreated *K. pneumoniae*, *S. aureus* and *M. luteus* cells are consistent with other AFM studies (Fig. 8a, c, e) [13,54]. In contrast, on bacterial cells treated with the AgFAP3 nanoparticles can seen the great damage, which resulting in the release of their cellular contents into the surrounding environment (Fig. 8b, d, f). In our previous work was noticed a similar lysing effects of Ag-doped hydroxyapatite nanoparticles on the morphology of *S. aureus* cells [13].

The mechanism of toxic Ag+ actions is very complex, includes dominant binding to —SH and —NH_2 groups of proteins from microorganism envelope changing the cell structure, permeability and inactivating proteins. The silver ions penetrate into the cell, inactivates various proteins and formation of sparingly soluble chloride causing inhibition of cell respiration. Their interaction with nucleic acids can affect on preventing replication and translation processes. The antibacterial mechanisms by which fluoride may interfere with bacterial metabolism include the inhibition of the glycolytic enzyme enolase, urease, catalase, and the proton-extruding ATPase [55,56]. In our study, according to ion realise, antibacterial and AFM studies, antibacterial mechanism action of AgFAP samples involves synergism of silver and fluoride ions. The action can associated with interaction bacterial cells envelope and Ag+ and F- ions released into the environment, as well as those ions present in the surface of nanoparticles. Antibacterial ions present in the surfaces of nanoparticle can be relatively easily release to contact with bacterial cells. Penetration of Ag+ and F- ions in the cellular envelope causes lysis of cells which leads to their death.

5. Conclusions

The present report described a simple process for the production of Ag^+- doped fluorapatite powders in aqueous medium. The analysis of XRD, FTIR and SEM showed that particles of silver-doped fluorapatite samples are of nano size and homogenous in composition. The synthesized AgFAP samples contain relatively low concentrations of silver ions were showed high antibacterial activity against *K. pneumoniea*, *S. aureus* and *M. luteus*. The result of this study, indicates that Ag-doped fluorapatite nanomaterials are promising as antibacterial biomaterials in orthopedics, dentistry and in the purification of waste water.

Acknowledgements

This work was supported by the Ministry of Education, Science and Technological Development of the Republic of Serbia (Project No. III 43009).

References

[1] S.V. Dorozhkin, Calcium orthophosphates in nature biology and medicine, Materials 2 (2009) 399–498.
[2] M. Mozafari, Bioceramics in the realm of history, Bioceram. Dev. Appl. (2014), http://dx.doi.org/10.4172/2090-5025.1000e106.
[3] D. Campoccia, L. Montanaro, C.R. Arciola, The significance of infection related to orthopedic devices and issues of antibiotic resistance, Biomaterials 27 (2006) 2331–2339.
[4] M. Mozafari, F. Moztarzadeh, Silver-doped bioactive glasses: What remains unanswered? Interceram 62 (2013) 423–425.
[5] F.M. Burke, N.J. Ray, R.J. McConnell Cork, Fluoride-containing restorative materials, Int. Dent. J. 56 (2006) 33–43.
[6] C. Van Loveren, The antimicrobial action of fluoride and its role in caries inhibition, J. Dent. Res. 69 (1990) 676–683.
[7] G.G. Craig, K.R. Powell, C.A. Price, Clinical evaluation of a modified silver fluoride application technique designed to facilitate lesion assessment in outreach programs, BMC Oral Health 13 (2013) 73.
[8] J.J.-Y. Peng, M.G. Botelho, J.P. Matinlinn, Silver compounds used in dentistry for caries management: A review, J. Dent. 40 (2012) 531–541.
[9] M. Glehr, A. Leithner, J. Friesenbichler, W. Goessler, A. Avian, D. Andreou, W. Maurer-Ertl, R. Windhager, P.-U. Tunn, Argyria following the use of silver-coated megaprostheses: No association between the development of local argyria and elevated silver levels, Bone Joint J. 95–B (2013) 988–992.
[10] N. Hadrupa, H.R. Lam, Oral toxicity of silver ions, silver nanoparticles and colloidal silver–A review, Regul. Toxicol. Pharmacol. 68 (2014) 1–7.
[11] Ž. Radovanović, B. Jokić, D. Veljović, S. Dimitrijević, V. Kojić, R. Petrović, D. Janacković, Antimicrobial activity and biocompatibility of Ag^+- and Cu^{2+}-doped biphasic hydroxyapatite/α-tricalcium phosphate obtained from hydrothermally synthesized Ag^+- and Cu^{2+}-doped hydroxyapatite, Appl. Surf. Sci. 307 (2014) 513–519.
[12] S. Jadalannagari, K. Deshmukh, S.R. Ramanan, M. Kowshik, Antimicrobial activity of hemocompatible silver doped hydroxyapatite nanoparticles synthesized by modified sol–gel technique, Appl. Nanosci. 4 (2014) 133–141.
[13] V. Stanić, D. Janaćković, S. Dimitrijević, S.B. Tanasković, M. Mitrić, M.S. Pavlović, A. Krstić, D. Jovanović, S. Raičević, Synthesis of antimicrobial monophase silver doped hydroxyapatite nanopowders for bone tissue engineering, Appl. Surf. Sci. 257 (2011) 4510–4518.
[14] K. Yamagishi, K. Onuma, T. Suzuki, F. Okada, J. Tagami, M. Otsuki, P. Senawangse, Materials chemistry: a synthetic enamel for rapid tooth repair, Nature 453 (2005) 819.
[15] L. Wang, S. He, X. Wu, S. Liang, Z. Mu, J. Wei, F. Deng, Y. Deng, S. Wei, Polyetheretherketone/nano-fluorohydroxyapatite composite with antimicrobial activity and osseointegration properties, Biomaterials 35 (2014) 6758–6775.
[16] X. Ge, Y. Leng, C. Bao, S.L. Xu, R. Wang, F. Ren, Antibacterial coatings of fluoridated hydroxyapatite for percutaneous implants, J. Biomed. Mater. Res. A 95 (2010) 588–599.
[17] N. Montazeri, R. Jahandideh, E. Biazar, Synthesis of fluorapatite–hydroxyapatite nanoparticles and toxicity investigations, Int. J. Nanomed. 6 (2011) 197–201.
[18] V. Stanić, S. Dimitrijević, D.G. Antonović, B.M. Jokić, S.P. Zec, S.T. Tanasković, S. Raičević, Synthesis of fluorine substituted hydroxyapatite nanopowders and application of the central composite design for determination of its antimicrobial effects, Appl. Surf. Sci. 290 (2014) 346–352.

[19] S. Overgaard, K. Søballe, M.C. Lind, C. Bünger, Resorption of hydroxyapatite and fluorapatite coatings in man. An experimental study in trabecular bone, J. Bone Joint Surg. Br. 79 (1997) 654–659.
[20] S. Jantová, M. Theiszová, S. Letasiová, L. Birosová, T.M. Palou, In vitro effects of fluor-hydroxyapatite, fluorapatite and hydroxyapatite on colony formation, DNA damage and mutagenicity, Mutat. Res. 652 (2008) 139–144.
[21] J. Wei, J. Wang, W. Shan, X. Liu, J. Ma, C. Liu, J. Fang, S. Wei, Development of fluorapatite cement for dental enamel defects repair, J. Mater. Sci.: Mater. Med. 22 (2011) 1607–1614.
[22] A. Forghani, M. Mapar, M. Kharaziha, M. d H. Fathi, Novel fluorapatite-forsterite nanocomposite powder for oral bone defects, Int. J. Appl. Ceram. Technol. 10 (2013) E282–E289.
[23] J. Kolmas, E. Groszyk, D. Kwiatkowska-Róhycka, Substituted hydroxyapatites with antibacterial properties, BioMed. Res. Int. 2014 (2014) 178123.
[24] D. Gopi, S. Ramya, D. Rajeswari, P. Karthikeyan, L. Kavitha, Strontium, cerium co-substituted hydroxyapatite nanoparticles: Synthesis, characterization, antibacterial activity towards prokaryotic strains and in vitro studies, Colloids Surf. A 451 (2014) 172–180.
[25] V. Stanić, S. Dimitrijević, J. Antić-Stanković, M. Mitrić, B. Jokić, I.B. Plećaš, S. Raičević, Synthesis, characterization and antimicrobial activity of copper and zinc-doped hydroxyapatite nanopowders, Appl. Surf. Sci. 256 (2010) 6083–6089.
[26] Y. Yan, X. Zhang, Y. Huang, Q. Ding, X. Pang, Antibacterial and bioactivity of silver substituted hydroxyapatite/TiO2 nanotube composite coatings on titanium, Appl. Surf. Sci. 314 (2014) 348–357.
[27] M. Honda, Y. Kawanobe, K. Ishii, T. Konishi, M. Mizumoto, N. Kanzawa, M. Matsumoto, M. Aizawa, In vitro and in vivo antimicrobial properties of silver-containing hydroxyapatite prepared via ultrasonic spray pyrolysis route, Mater. Sci. Eng. C 33 (2013) 5008–5018.
[28] B. Ye, K. Cui, Q.L. Feng, G.Q. Chen, F.Z. Cui, Synthesis and high temperature resistance properties of silver loaded fluorapatite antibacterial, J. Inorg. Mater. 18 (2003) 485–489.
[29] M. Turkoz, A.O. Atilla, Z. Evis, Silver and fluoride doped hydroxyapatites: Investigation by microstructure, mechanical and antibacterial properties, Ceram. Int. 39 (2013) 8925–8931.
[30] F. Bir, H. Khireddine, A. Touati, D. Sidane, S. Yala, H. Oudadesse, Electrochemical depositions of fluorohydroxyapatite doped by Cu^{2+}, Zn^{2+}, Ag^{+} on stainless steel substrates, Appl. Surf. Sci. 258 (2012) 7021–7030.
[31] M.P. Reddy, A. Venugopal, M. Subrahmanyam, Hydroxyapatite-supported Ag–TiO_2 as Escherichia coli disinfection photocatalyst, Water Res. 41 (2007) 379–386.
[32] H. Chen, K. Sun, Z. Tang, R.V. Law, J.F. Mansfield, A. Czajka-Jakubowska, B.H. Clarkson, Synthesis of fluorapatite nanorods and nanowires by direct precipitation from solution, Cryst. Growth Des. 6 (2006) 1504–1508.
[33] V. Jokanović, B. Čolović, N. Jović, B. Babić-Stojić, B. Jokanović, Mechanochemical and low-temperature synthesis of nanocrystalline fluorohydroxyapatite/fluorapatite, Int. J. Appl. Ceram. Technol. 10 (2013) 957–969.
[34] M. Nabiyouni, H. Zhou, T.J.F. Luchini, S.B. Bhaduri, Formation of nanostructured fluorapatite viamicrowave assisted solution combustion synthesis, Mater. Sci. Eng. C 37 (2014) 363–368.
[35] S. Loher, W.J. Stark, M. Maciejewski, A. Baiker, S.E. Pratsinis, D. Reichardt, F. Maspero, F. Krumeich, D. Günther, Fluoro-apatite and calcium phosphate nanoparticles by flame synthesis, Chem. Mater. 17 (2005) 36–42.
[36] J. Zhao, X. Dong, M. Bian, J. Zhao, Y. Zhang, Y. Sun, J.H. Chen, X.H. Wang, Solution combustion method for synthesis of nanostructured hydroxyapatite, fluorapatite and chlorapatite, Appl. Surf. Sci. 314 (2014) 1026–1033.
[37] I. Smičiklas, A. Onjia, S. Raičević, Experimental design approach in the synthesis of hydroxyapatite by neutralization method, Sep. Purif. Technol. 44 (2005) 97–102.
[38] W. Kraus, G. Nolze, POWDER CELL - a program for the representation and manipulation of crystal structures and calculation of the resulting X-ray powder patterns, J. Appl. Cryst. 29 (1996) 301–303.
[39] I. Rehman, W. Bonfield, Characterization of hydroxyapatite and carbonated apatite by photo acoustic FTIR spectroscopy, J. Mater. Sci.: Mater. Med. 8 (1997) 1–4.
[40] I.R. Gibson, W. Bonfield, Novel synthesis and characterization of an AB-type carbonate-substituted hydroxyapatite, J. Biomed. Mater. Res. 59 (2002) 697–708.
[41] Z.H. Cheng, A. Yasukawa, K. Kandori, T. Ishikawa, FTIR study on incorporation of CO_2 into calcium hydroxyapatite, J. Chem. Soc. Faraday Trans. 94 (1998) 1501–1505.
[42] M. Jemal, I. Khattech, Simultaneous thermogravimetry and gas chromatography during decomposition of carbonate apatites, Thermochim. Acta 152 (1989) 65–76.
[43] F.B. Ayed, J. Bouaziz, K. Bouzouita, Pressureless sintering of fluorapatite under oxygen atmosphere, J. Eur. Ceram. Soc. 20 (2000) 1069–1076.
[44] K. Tõnsuaadu, K.A. Gross, L. Plūduma, M. Veiderma, A review on the thermal stability of calcium apatites, J. Therm. Anal. Calorim. 110 (2012) 647–659.
[45] S. Lazić, Microcrystalline hydroxyapatite formation from alkaline solutions, J. Cryst. Growth 147 (1995) 147–154.
[46] M. Vallet-Regí, I. Izquierdo-Barba, M. Colilla, Structure and functionalization of mesoporous bioceramics for bone tissue regeneration and local drug delivery, Phil. Trans. R. Soc. A 370 (2012) 1400–1421.
[47] S.V. Dorozhkin, A review on the dissolution models of calcium apatites, Prog. Cryst. Growth Charact. Mater. 44 (2002) 45–61.
[48] C.F. Lord, M.C. Gebhardt, W.W. Tomford, H.J. Mankin, Infection in bone allografts, J. Bone Jt. Surg. 70A (1988) 369–376.
[49] L.G. Harris, R.G. Richards, Staphylococci and implant surfaces: a review, Injury 37 (2006) S3–S14.
[50] M.M. Tunney, G. Ramage, S. Patrick, J.R. Nixon, P.G. Murphy, S.P. Gorman, Antimicrobial susceptibility of bacteria isolated from orthopedic implants following revision hip surgery, Antimicrob. Agents Chemother. 42 (1998) 3002–3005.
[51] Y.H. An, R.J. Friedman, Concise review of mechanisms of bacterial adhesion to biomaterial surfaces, J. Biomed. Mater. Res. B 43 (1998) 338–348.
[52] H.C. Syed, M. Ravaoarinoro, LiF reduces MICs of antibiotics against clinical isolates of Gram-positive and Gram-negative bacteria, Int. J. Microbiol. 2012 (2012) 454065.
[53] C.S. Ciobanu, S.L. Iconaru, P.L. Coustumer, L.V. Constantin, D. Predoi, Antibacterial activity of silver-doped hydroxyapatite nanoparticles against gram-positive and gram-negative bacteria, Nanoscale Res. Lett. 7 (2012) 324.
[54] A. Zdybicka-Barabas, B. Januszanis, P. Mak, M. Cytryńska, An atomic force microscopy study of Galleria mellonella apolipophorin III effect on bacteria, Biochim. Biophys. Acta 1808 (2011) 1896–1906.
[55] R.E. Marquis, S.A. Clock, M. Mota-Meira, Fluoride and organic weak acids as modulators of microbial physiology, FEMS Microbiol. Rev. 26 (2003) 493–510.
[56] A. Wiegand, W. Buchalla, T. Attin, Review on fluoride-releasing restorative materials–Fluoride release and uptake characteristics, antibacterial activity and influence on caries formation, Dent. Mater. 23 (2007) 343–362.